Competition between bulk and interface plasmonic modes in valence electron energy-loss spectroscopy of ultrathin SiO_2 gate stacks

M. Couillard,* A. Yurtsever, and D. A. Muller
Applied and Engineering Physics, Cornell University, Ithaca, New York 14853, USA
(Received 17 September 2007; published 26 February 2008)

Low-energy excitations ($\lesssim$50 eV) induced by fast electrons in materials can exhibit a collective and delocalized nature. Here, we study such excitations in $Si/SiO_2/Si$ stacks by spatially resolved electron energy-loss spectroscopy with a sub-2 Å electron beam. Experimental spectra acquired in the SiO_2 layer are found to display delocalized contributions originating from interface plasmons, interband transitions, and Čerenkov radiation. A comparison with simulations based on a local semiclassical dielectric model, which includes relativistic effects, highlights the changes in interface plasmon coupling as the thickness of the central SiO_2 layer is reduced. We demonstrate both experimentally and theoretically that when the electron probe is located at the center of a 2 nm SiO_2 layer, the optical response expected from a bulk SiO_2 layer is suppressed and delocalized contributions dominate. As the layer thickness is reduced, the spectra become more like that of bulk Si even if the incident electrons travel only in the SiO_2 layer. This poses a major challenge for directly extracting local optical properties of ultrathin layers by electron energy-loss spectroscopy.

DOI: 10.1103/PhysRevB.77.085318 PACS number(s): 73.20.Mf, 68.37.Lp, 79.20.Uv, 81.07.−b

I. INTRODUCTION

Thin dielectric layers comprising the gate stacks of field-effect transistors are the narrowest features in integrated circuits. They have widths that now reach well below 2 nm. Determining the physical and electronic properties of these layers and their neighboring interfaces therefore represents a major challenge.[1] Electron energy-loss spectroscopy (EELS) performed in a scanning transmission electron microscope (STEM) provides sufficient spatial resolution to study locally the nature of electronic excitations in these stratified systems.[2,3] Two main energy-loss categories are usually considered. Core excitations at high energies, where electrons are excited from deep atomic levels to the valence band, have been used extensively in spatially resolved experiments to access the electronic properties[2,3] and to map elements and chemical phases in gate stacks.[4–8] Valence losses, which explore excitations with initial level near the Fermi energy, provide local band structure information, but also include radiative losses and collective excitations such as plasmons.[9] Because they are less easily interpretable, low-loss spectra have not been used as extensively to probe gate stacks. Previous studies of Si/SiO_2 interfaces have identified a strong spectral feature around 8 eV (below the SiO_2 band gap energy) originating from an interface plasmon,[10–14] and have also reported changes at higher energy loss.[15,16]

Delocalized signals, originating from the excitation of modes located relatively far from the electron trajectory, contribute to valence EELS.[17,18] An estimate of the characteristic delocalization length is given by the Bohr's adiabatic criterion,[19,20] which gives an upper limit on the impact parameter for efficient energy transfer $b_{max} \sim v/\omega$, where v is the speed of the incident electron and ω is the frequency associated with the excited mode. The impact parameter b_{max} marks the crossover between the near-field[21] and far-field couplings of the probe to the sample. For nonradiative modes, the signal will decay exponentially at impact parameters $b > b_{max}$. For radiative modes, the signal will decay, with the power law of the multipole being excited.[20] When the dimensions of the sample become comparable to b_{max}, a significant departure from the bulk energy function can be expected.

Valence losses depend strongly on the geometry of the sample under study.[22–26] For instance, an electron traveling close to a planar boundary between two different media may excite an interface plasmon (IP). It consists of a collective oscillation of quasi-free-electrons, like the bulk plasmon, except that the IP is confined near an interface.[9] Such delocalized losses may produce features below the band gap energy of insulators. IP losses may therefore impose a limit on the direct evaluation of band gap energies by EELS, an approach that has previously been applied successfully to bulk materials[27] and freestanding nanostructures.[28]

In layered systems of finite dimensions, IPs associated with different interfaces may interact. For a metallic slab surrounded by vacuum, oscillations at the two surfaces will couple significantly when the layer width d is such that $k_p d \ll 1$ (for $k_p = \omega_p/c$, where ω_p is the bulk plasmon frequency and c is the speed of light in vacuum).[9] More generally, such a coupling breaks the dispersion curve degeneracy of interface plasmons at scattering vectors k lower than $1/d$. When a system consists of several layers, loss spectra will then depend on the interaction between all interface modes as well as on the trajectory of the incident electrons.[10,29,30]

The velocity of incident electrons in EELS experiments typically exceed half the speed of light. Consequently, a complete description of valence losses requires a relativistic treatment. This can be achieved by solving the complete set of Maxwell equations in the presence of an incident electron. With this approach, the dispersion of IPs, i.e., the change in energy as a function of the scattering vector k, is properly described.[30] Moreover, because energy-loss spectra entail an integration over k, the shape of a feature associated with an interface mode is dependent on its dispersion. In addition, the dispersion also accounts for the variation of an IP feature in spectra acquired at different impact parameters.

An important consequence of including relativistic effects is the description of energy loss by excitation of radiative modes. Of particular importance in EELS studies of semiconductors and insulators (e.g., silicon and silica) is the emission of Čerenkov radiation. This effect occurs when electrons travel through or in the vicinity of a medium with a velocity v larger than the speed of light in that medium ($v > c/n$, where n is the refractive index of the medium).[20] Čerenkov losses usually occur in high-n materials at energies below the optical gap onset, thereby affecting band gap measurements.[31–34] Because of its radiative nature, Čerenkov losses depend on the specimen geometry over a long range.[35] In particular, total internal reflections at interfaces can confine the radiation in a slab, such as a typical TEM specimen, and produce waveguide modes.[36–39]

In this paper, we explore the influence of the SiO_2 layer width on valence EELS spectra for gate stacks consisting of Si/SiO_2/poly-Si. Two configurations, with SiO_2 layer widths of 10 and 2 nm, are studied. Experimental results are compared with simulations based on a relativistic local dielectric model developed by Bolton and Chen.[29] This comparison provides a basis for interpretation of delocalized signals, which have been assigned to three categories: interband transitions, interface plasmons, and Čerenkov radiation. It also allows for an understanding of interface coupling effects in the energy loss of electrons. In particular, our results demonstrate that a spectrum acquired with the electron probe located in the SiO_2 layer will tend toward the one for bulk Si as the SiO_2 layer becomes very thin.

II. EXPERIMENTS

Annular dark field (ADF) STEM images of the two gate stacks studied are shown in Fig. 1 (top). The SiO_2 layer is 10 nm thick in the first case (left) and 2 nm in the second (right). Deposition conditions are described in Ref. 2. The poly-Si capping layer deposited on the 2 nm SiO_2 layer was annealed at 1050 °C for 10 s, producing a sharper interface. ADF imaging was performed in a 200 kV FEI Tecnai F20-ST STEM with a convergence and a collection semiangle of 10 and 50 mrad, respectively. The estimated probe current is 10–20 pA. The electron microscope is fitted with a monochromator and a Gatan imaging filter 865-ER, which was operated with an acceptance semiangle of 25 mrad for the spatially resolved EELS presented here. The stability associated with the monochromator system (used in the unfiltered mode in the experiments presented in this paper) enhances the EELS energy resolution, which was evaluated as ~0.5 eV. Line scans displayed in Fig. 1 (bottom) for the 10 nm layer (left) and the 2 nm layer (right) have a step size of 4 and 2 Å and an acquisition time of 1 and 0.5 s, respectively. The intense zero loss peak (ZLP) was blocked out using the energy-selecting slit in the spectrometer. An extension of the ZLP tail is visible at low energies.

Spectra acquired at the center of the two SiO_2 layers (dotted curves in Fig. 1) differ considerably. To emphasize this result, spectra acquired ~1 nm away from the interface with the Si substrate are presented in Fig. 2 for the two layered systems discussed. These spectra are compared with a bulk

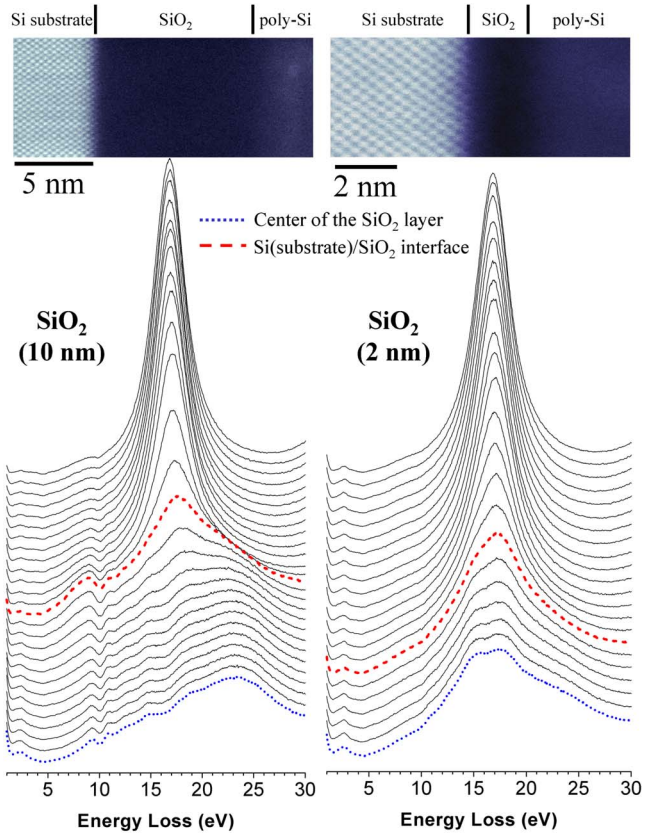

FIG. 1. (Color online) ADF images (top) and EELS line scans (bottom) for two Si/SiO_2/poly-Si gate stacks. The widths of the SiO_2 layer are 10 nm (left) and 2 nm (right). Step sizes and specimen thicknesses were ~4 Å and 110 nm for the line scan on the left and ~2 Å and 105 nm for the line scan on the right. Both line scans start in the Si substrate (top spectra).

SiO_2 spectrum in Fig. 2(a) and with a spectrum acquired beside a single isolated Si/SiO_2 interface in Fig. 2(b). For the thinnest layer, the bulk SiO_2 plasmon at ~23 eV is clearly suppressed and a shift of intensity toward the bulk Si plasmon at 16.7 eV is observed. Below the SiO_2 band gap energy (9.9 eV), a strong IP is clearly visible for the single interface and also for the 10 nm system at slightly higher energy loss [Fig. 2(b)]. For the 2 nm gate stack, the IP feature and the interband transition at ~10.8 eV become hard to distinguish. A peak below 4 eV that is visible in the three spectra is associated with the emission of Čerenkov radiation. In this instance, Čerenkov radiation is emitted in Si by fast electrons traveling in SiO_2, as discussed in the next section.

EELS line scans shown in Fig. 1 were acquired in relatively thick regions of the specimens in order to reduce contributions from the modes associated with the entrance and exit surfaces (i.e., interfaces between the vacuum and the specimen). Specimen thicknesses were evaluated with the method described in Ref. 40, with a mean-free path for incident electrons in Si of 134 nm for our experimental conditions. The extracted values are 110 nm for the line scan on the left and 105 nm for the line scan on the right, values that are considerably higher than those for a typical core-loss analysis.

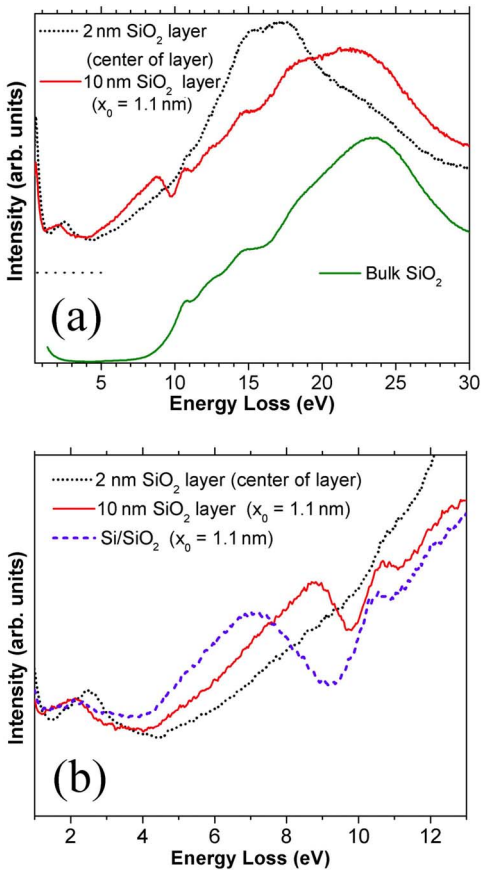

FIG. 2. (Color online) (a) Loss spectra acquired ~1 nm away from the Si substrate for two gate stacks (top) with SiO_2 layer widths of 2 and 10 nm, along with a bulk SiO_2 spectrum (bottom). (b) is a closeup view of the spectra for the gate stacks in (a), along with a spectra acquired near an isolated Si/SiO_2 interface. Specimen thicknesses were the same as in Fig. 1 for the gate stacks and 110 nm for the Si/SiO_2 sample.

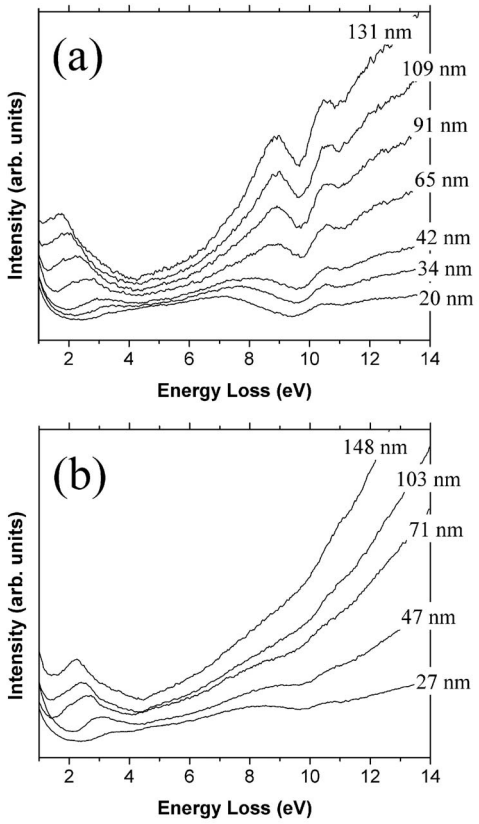

FIG. 3. Spectra acquired at the center of the SiO_2 layers for different specimen thicknesses. Results for (a) a gate stack with a 10 nm SiO_2 layer and (b) for a stack with a 2 nm layer.

In Fig. 3, we present spectra acquired at the center of the SiO_2 layers [(a) 10 nm layer; (b) 2 nm layer] for different specimen thicknesses. As the probed region becomes thinner, two major changes occur. First, the IP feature broadens and shifts to lower energies. This is attributed to contributions from modes confined near the junctions between the Si/SiO_2 interface and the specimen surfaces running perpendicularly.[41] A second variation is the blueshift of the Čerenkov peak. A similar behavior has previously been observed experimentally for electrons traversing Si slabs.[34] Because of total internal reflections at the (Si/vacuum) specimen surfaces, these radiative excitations should be interpreted in terms of waveguide modes.[36–39] The dependence of the peak position on energy occurs because of a low-frequency cutoff dependent on the Si slab thickness. For the first symmetric mode, this cutoff corresponds to an energy of $\pi\hbar c/(L\sqrt{\epsilon-1})$, where L is the specimen thickness and ϵ is the dielectric constant of the medium. Taking $\epsilon_{Si}=11.9$ and $L=100$ nm, this gives an energy cutoff of ~2 eV, corresponding approximately to the drop in intensity observed in Fig. 2 for the Čerenkov peak.

For very thick specimens, beam broadening is expected to affect loss spectra, especially for gate stacks with ultrathin layers. However, as will be demonstrated in the next sections, the strong effects observed in Fig. 1 for the 2 nm SiO_2 system are predominantly due to delocalized excitations.

III. SIMULATIONS

In order to understand the substantial changes observed in experimental spectra as the SiO_2 layer becomes thinner, we use a local relativistic dielectric formalism to model the loss signal. The local response approximation, which neglects nonlocal dispersive effects,[42,43] was first proposed by Fermi[44] and is usually justified at high velocities. This approach is valid at low momentum transfer and might therefore require modifications for EELS experiments performed with a large collection aperture or for spectra acquired with a probe in close proximity to an interface. The model used here was developed by Bolton and Chen[29] for stratified systems composed of any number of layers. Using complex dielectric constants of bulk materials as input parameters, this approach simulates spectra for various layer widths and probe positions. Dielectric constants for Si and SiO_2 were taken from optical data tabulated in Ref. 45. We define the coordinates as shown in Fig. 4: Incident electrons travel along the z direction at a distance x_0 from the interface with the Si substrate. The model neglects the convergence and the scattering angles of incident electrons and assumes an infinite thickness along z. Thus, because of the last approximation, the wave-

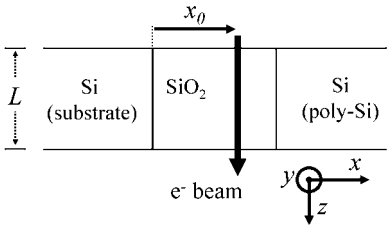

FIG. 4. Schematic view of the gate stack.

guide modes discussed above are not described with this approach.

The energy-loss probability density per unit path length for transferring energy $\hbar\omega$ and y-momentum $\hbar k_y$ is given according to Bolton and Chen[29] by

$$\frac{d^3P}{d\omega dk_y dz} = \frac{e^2}{4\pi^2\varepsilon_0\hbar v^2}\,\mathrm{Im}\{\chi_m^{(n)}\}. \tag{1}$$

The superscript n of the loss function χ indicates the number of layers in the system and the subscript m refers to the layer where the probe is located. k_y is the component of the scattering vector along the y axis, v is the speed of the incident electrons, e is the elementary electric charge, ε_0 is the vacuum permittivity, and $\hbar$ is Planck's constant. Equation (1) gives the loss probability as a function of the energy $(\hbar\omega)$ and k_y. To obtain a spectrum, an integration over k_y is performed with an upper limit corresponding to the EELS collection aperture of 25 mrad. Note that k_x is implicitly integrated from 0 to ∞; therefore, the results do not account for the circular shape of the EELS aperture. A complete formula with an upper limit on both k_x and k_y is given in Ref. 12 for a single interface. A correction for layered systems is proposed in the next section of the present paper.

Because of the local approximation, it is possible to separate the bulk and interface contributions $(\chi_{\text{total}}=\chi_{\text{bulk}}+\chi_{\text{interface}})$. The latter gives the so-called delocalized signal. This decomposition is particularly apparent for the case of a single interface. In the formalism of Bolton and Chen,[29] this corresponds to $n=0$ layer, and the equation reduce to the one derived by García-Molina *et al.*[46] For an interface between materials A and B, when the electron probe is located in B, the loss function is expressed as

$$\chi_B^{(0)} = -\frac{1-\epsilon_B(v/c)^2}{\epsilon_B q_B} + \frac{1-\epsilon_B(v/c)^2}{\epsilon_B q_B}e^{-2q_B x_0} + 2e^{-2q_B x_0}\left\{-\frac{1}{h_{\text{BA}}^+} + \frac{(v/c)^2}{\tilde{h}_{\text{BA}}^+}\right\}, \tag{2}$$

where

$$q_j = \sqrt{k_y^2 + \left(\frac{\omega}{v}\right)^2 - \epsilon_j\left(\frac{\omega}{c}\right)^2},$$

$$h_{BA}^{\sigma} = q_B\epsilon_A + \sigma q_A\epsilon_B,$$

$$\tilde{h}_{BA}^{\sigma} = q_B + \sigma q_A.$$

ϵ_A and ϵ_B are the complex dielectric constants of the two media and x_0 is the impact parameter taken with respect to the A/B interface. In this paper, A is Si and B is SiO_2. The first term in Eq. (2) corresponds to the bulk contribution and includes relativistic effects such as Čerenkov losses. A bulk plasmon is expected close to the energy where $\mathrm{Re}(\epsilon_B)=0$. Delocalized contributions are given by the other terms with a dependence on x_0. The second term in Eq. (2) takes exactly the same form as the bulk component, except for the opposite sign in front and an exponential that decreases as the probe moves away from the interface. This indicates that the intensity for interface modes is taken away from the bulk one (the Begrenzung effect).[47] Finally, the last term produces features characteristic of interface modes. In the classical limit $(c\to\infty)$, the bulk term reduces to the well known loss function $-1/\epsilon_B$, and the last interface term takes the form of $-2/(\epsilon_A+\epsilon_B)$, where a strong IP is expected when $\mathrm{Re}(\epsilon_A+\epsilon_B)=0$.

A simulated spectrum for an electron traveling in SiO_2 at $x_0=1$ nm from a single Si/SiO_2 interface [Fig. 5(a)] displays a strong IP around 8 eV, below the SiO_2 gap at 9.9 eV. As evident from Fig. 5(a), the shape of this feature is strongly affected by retardation effects. Also, for a spectrum simulated in the classical limit, the loss signal drops sharply below the Si direct gap at 3.4 eV and eventually reaches 0 at the Si indirect gap of 1.1 eV. In contrast, a relativistic approach predicts Čerenkov contributions in that energy range.

The origin of the features just described is better understood with the simulated loss image presented at the bottom of Fig. 5(a), which displays the loss probability as a function of k_y and the energy. In this case, the vertical k_y axis runs from 0 to 0.38 nm^{-1}, which correspond to a scattering angle of 150 μrad. Therefore, only scattering angles much lower than the EELS acceptance semiangle are displayed. Nevertheless, the low-k_y region is the most intense part of the loss image. A strong momentum dispersion of the IP is observed in the image of Fig. 5(a). As this effect is only properly described relativistically, it explains the difference in the shape of the spectra simulated with and without retardation effects. Incident electrons traveling in SiO_2 generate Čerenkov radiation in both Si and SiO_2, as indicated in the loss image. The former produces a more important contribution and gives rise to a plateau in the simulated spectrum at low energies (<3.4 eV). It should be emphasized that here, the Čerenkov radiation in Si is induced by fast electrons traveling in SiO_2. Interband transitions (IBs) in SiO_2 appear, as indicated, above the 9.9 eV onset. In addition, IBs in Si are also present. They are superimposed on the main IP in the spectrum and appear as dim vertical streaks in the loss image at energies indicated by the three vertical lines. Note that the dispersion in the band structure is not included in this model, and therefore IBs appear as straight lines.

For a layered system with a symmetric $A/B/A$ arrangement, the loss function is complicated by the interaction between the A/B interface modes. With a probe located in B, the function is given by[29]

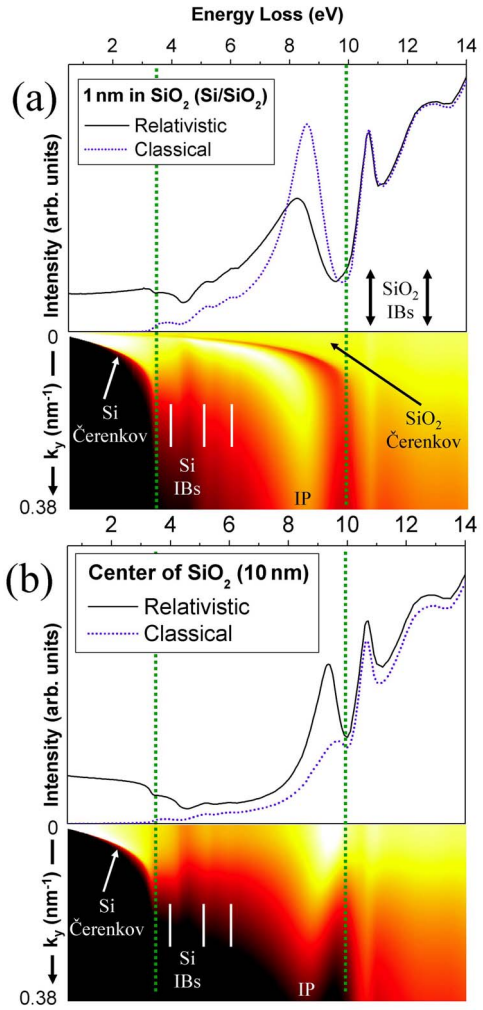

FIG. 5. (Color online) Simulated spectra and E-k_y loss images for (a) a single Si/SiO_2 interface with the probe located 1 nm from the Si substrate and (b) a $Si/SiO_2/Si$ system with the probe located at the center of the 10 nm SiO_2 layer. For the loss images, the energy (horizontal axis) extends from 0.5 to 14 eV and k_y (vertical axis) extends from 0 to 0.38 nm^{-1} (corresponding to a scattering angle of 150 μrad). Vertical dotted lines indicate the onset position of the SiO_2 gap at 9.9 eV and the Si direct gap at 3.4 eV. Loss images include relativistic effects, and their intensity is plotted on a logarithmic scale.

$$\chi_B^{(1)} = \frac{1}{q_B \epsilon_B k^2}\left\{\epsilon_B k_y^2 \left(\frac{v}{c}\right)^2 \frac{\tilde{\gamma}^- \tilde{\zeta}^+}{[\tilde{L}^+\tilde{L}^-]} - q_B^2 \frac{\gamma^+ \zeta^-}{[L^+L^-]}\right\}, \qquad (3)$$

where

$$\gamma^\sigma = h_{BA}^+ e^{q_B(2d-x_0)} - \sigma h_{BA}^- e^{q_B x_0},$$

$$\zeta^\sigma = h_{BA}^+ e^{q_B x_0} + \sigma h_{BA}^- e^{-q_B x_0},$$

$$L^\sigma = h_{BA}^+ e^{q_B d} + \sigma h_{BA}^-.$$

k is the scattering wave vector $[k^2=(\omega/v)^2+k_y^2]$, and d is the width of layer B. To obtain the tilded terms (e.g., $\tilde{L}$), we replace h_{BA}^σ by $\tilde{h}_{BA}^\sigma$ in all the definitions. Strong modes are expected when $[L^+L^-][\tilde{L}^+\tilde{L}^-]\to 0$. $[L^+L^-]$ is associated with transverse magnetic (TM) modes, whereas $[\tilde{L}^+\tilde{L}^-]$ is associated with transverse electric modes. TM modes are found to dominate the loss signal. Because of the symmetry of the $A/B/A$ system studied (i.e., $Si/SiO_2/Si$), it is also possible to differentiate between modes symmetric ($L^+=0$) and antisymmetric ($L^-=0$) in their charge distribution.[29]

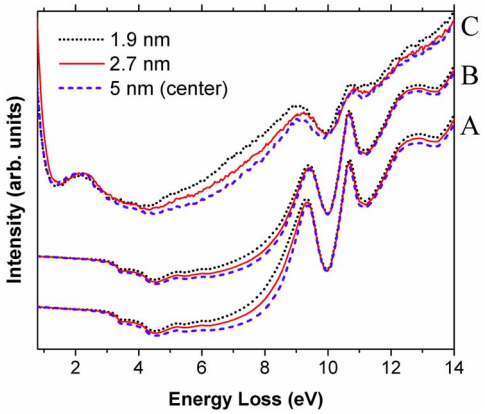

FIG. 6. (Color online) Experimental spectra (C) acquired in the 10 nm SiO_2 layer for x_0=1.9, 2.7, and 5 nm, taken with respect to the interface with the Si substrate. The corresponding simulated spectra were done without (A) and with (B) extra SiO layers at the interfaces (see text). The effect of the SiO layers is to damp slightly the interface plasmon modes.

Figure 5(b) presents a simulated spectrum along with its associated loss image for a $Si/SiO_2/Si$ system, where the probe is located at the center of the 10 nm SiO_2 layer. A modification of the k_y dispersion of IPs due to coupling effects is found to shift the IP feature to higher energy losses in the spectra. In contrast, Si and SiO_2 IB features remain at the same position. Čerenkov radiation in SiO_2 is suppressed because of the finite layer width. On the contrary, the signal associated with Čerenkov radiation in Si is slightly increased. Again, the relativistic simulation differs considerably from the classical one.

IV. DISCUSSION

IP coupling affects the energy-loss spectra acquired in both gate stacks shown in Fig. 1. The difference in IP dispersion between the simulated loss images of Figs. 5(a) and 5(b) is an indication of such an interaction between interface modes. In this section, we will first discuss coupling effects on energy loss for the case of a 10 nm SiO_2 layer, and then for a 2 nm layer.

A. 10 nm SiO_2 layer

For the system with a 10 nm layer, delocalized contributions affect the spectra mainly at low energies. Curves C in Fig. 6 present the dependence of experimental spectra on the impact parameter x_0, taken with respect to the interface with the Si substrate. A change in the shape of the IP feature is observed, displaying a relative increase in intensity below

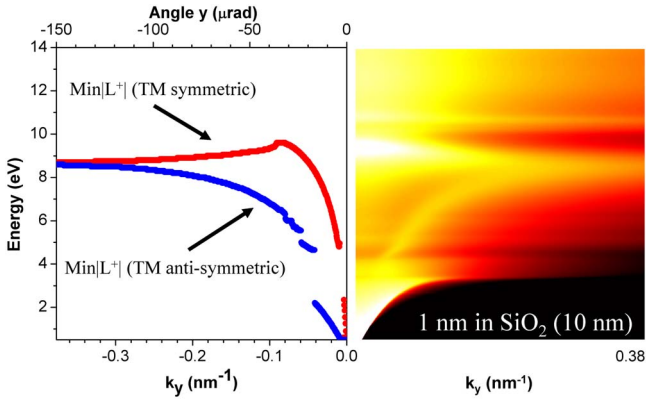

FIG. 7. (Color online) Right: Simulated E-k_y loss images for the Si/(10 nm)-SiO_2/Si stack with the probe located 1 nm away from the Si substrate. Left: Minimum in the $|L^+|$ and $|L^-|$ functions for the same system. The vertical energy axis extends from 0.5 to 14 eV, and the horizontal k_y axis extends from 0 to 0.38 nm^{-1} (corresponding to a scattering angle of 150 μrad). The intensity of the loss image is plotted on a logarithmic scale.

~9 eV as x_0 decreases. This is reproduced by the theory (A in Fig. 6). For these simulations, ϵ for the polycrystalline Si capping layer was approximated to be the same as for crystalline Si. As previously demonstrated, interdiffusion and roughness at the interface affect the shape of the IP feature in spectra acquired near a single isolated Si/SiO_2 interface.[12] To explore these effects, we follow Ref. 12 and incorporate an additional SiO layer (width of 5 Å) at the two Si/SiO_2 boundaries. The width of the SiO_2 layer is then reduced to 9 nm. In contrast to the case of a single isolated Si/SiO_2 interface, inserting suboxide layers in a Si/(10 nm)-SiO_2/Si system (B in Fig. 6) is found to have only a relatively small effect on the spectra.

A simulated E-k_y loss image for an electron trajectory located 1 nm away from the Si substrate is presented in Fig. 7 (right). The energy axis is now vertical, and no SiO layers were added for this simulation. The map displays two clear branches for the collective modes below the SiO_2 band gap energy. Mapping the minimum in $|L^+|$ and $|L^-|$ as a function of k_y (Fig. 7, left) allows for the assignment of the low-energy branch as an antisymmetric TM mode and the high-energy branch as a symmetric TM mode. Note that the curves at low k_y are not well defined; this is because bulk modes from Si and SiO_2 are also included in the condition $[L^{\pm}] \rightarrow 0$. Several local minima are therefore present in the $|L^{\pm}|$ functions, and only at high k_y do the minima correspond to the IP. The contribution from the antisymmetric component explains the increase in intensity below ~9 eV observed when the probe approaches the Si/SiO_2 interface. In fact, such a mode is completely absent when the probe is located at the center of the SiO_2 layer, as shown in the loss image of Fig. 5(b). Hence, a probe at the center of a symmetric system will only excite symmetric TM modes. Above the 9.9 eV gap onset, the model predicts contributions very similar to the ones for bulk SiO_2.

B. 2 nm SiO_2 layer

An experimental spectrum acquired at the center of the 2 nm SiO_2 layer is displayed in Fig. 8(a) (curve D). The

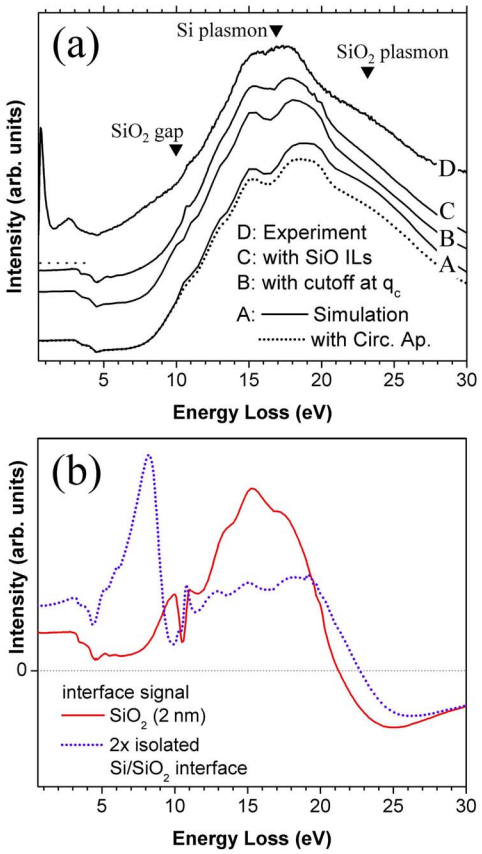

FIG. 8. (Color online) (a) Experimental and simulated (see text) spectra for an electron probe located at the center of the 2 nm SiO_2 gate stack. The spectra have been scaled with respect to their intensity maximum and shifted vertically for clarity (the short dotted line indicates the zero intensity for the experimental curve). (b) Delocalized interface contributions for the Si/(2 nm)-SiO_2/Si system, along with two times the contributions when a probe is located 1 nm away from an isolated Si/SiO_2 interface.

SiO_2 optical gap onset does not appear clearly in that case, and substantial changes are observed at higher energies. The bulk SiO_2 plasmon is no longer the prominent feature, and the intensity is increased in the energy region of the bulk Si plasmon. Those observations are partly reproduced in the simulated spectrum [curve A in Fig. 8(a)], although the model overestimates the contribution from the bulk SiO_2 plasmon and predicts an intensity maximum at a slightly higher energy loss than experimentally observed.

A first correction can be applied to take into account the circular shape of the EELS aperture. Since the bulk χ_{bulk} component dominates at high k, only this term will be modified. It is replaced by the bulk component given by Bolton and Chen[29] for normal incidence, where the cutoff in k corresponds exactly to the collection aperture. As can be seen in Fig. 8 (curve A, dotted line), this has only a small effect on the spectrum because of the high collection angle. A more important correction is introduced if we consider that the bulk plasmon is heavily damped above a wave vector q_c due to energy transfer to single electrons. With the formula in Ref. 40, we estimate that $q_c \sim 15$ nm^{-1} (6 mrad). Setting this value instead of the EELS aperture as the wave vector cutoff,

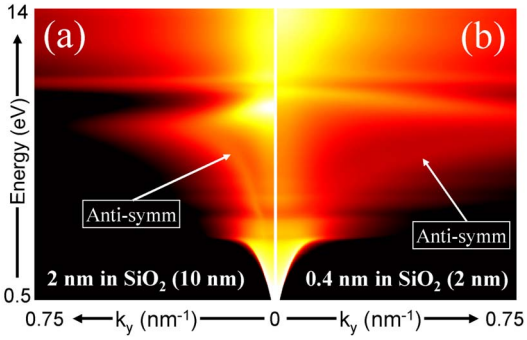

FIG. 9. (Color online) Simulated E-k_y loss images for (a) Si/(10 nm)-SiO_2/Si and (b) Si/(2 nm)-SiO_2/Si stacks. The electron probe is located at a distance x_0 equal to one-fifth of the layer widths. The energy extends from 0.5 to 14 eV, and k_y extends from 0 to 0.75 nm^{-1} (corresponding to a scattering angle of 300 μrad). The intensity is displayed on a logarithmic scale. Arrows point to the antisymmetric TM modes.

the simulated spectrum [curve B in Fig. 8(a)] is found to display a reduction in the contribution from the bulk SiO_2 plasmon but still fails to reproduce exactly the experimental results near the intensity maximum.

Finally, if we add an extra suboxide layer at each Si/SiO_2 boundary, producing a system with two 0.5 nm SiO layers and one 1 nm SiO_2 layer, the intensity maximum shifts slightly to lower energies [curve C in Fig. 8(a)], closer to the experimental value. The close agreement between experimental and simulated spectra suggests that the local response approximation, along with the correction to include the damping of the bulk plasmon above q_c, is adequate even for an ultrathin SiO_2 layer with a width of only 2 nm. Nonlocal dispersive effects,[42,43] not included in the present simulations beyond the q_c correction, are therefore expected to remain negligible as long as the probe is located far enough from the interfaces. Remaining discrepancies between experimental and theoretical curves are likely due to other approximations in the model, such as the description of the interfacial region and the oversight of the finite specimen thickness.

The clear departure of spectra acquired in the thin layer from the bulk SiO_2 spectrum is therefore attributed to the presence of the nearby interfaces, and not to a change in the electronic properties of the layer material. This can be better understood by looking at the delocalized $\chi_{\text{interface}}$ contributions. Figure 8(b) displays this signal for the Si/(2 nm)-SiO_2/Si system (full line) and compares it with two times the delocalized signal from an isolated Si/SiO_2 interface (dotted line). The latter corresponds to a hypothetical system where no interaction between IPs occurs. It is clear that coupling effects transfer the intensity from below the SiO_2 band gap to a region close to the Si bulk plasmon. Both curves become negative near the bulk SiO_2 plasmon energy. This corresponds to the Begrenzung effect mentioned in the previous section and explains the suppression of bulk modes.

To explain the observed variations for the IP feature below the SiO_2 gap onset, Fig. 9 presents E-k_y loss images for the two stacks studied. The impact parameter x_0 in this case is $\frac{1}{5}$ of the layer width, and the scattering angles go from 0 to 300 μrad. Two IP branches are predicted for both layer widths. At high k_y, the symmetric and antisymmetric modes converge toward ~8.5 eV. This occurs when $kd \sim 1$. It corresponds to $k_y \sim 0.1$ nm^{-1} for the 10 nm SiO_2 layer and to $k_y \sim 0.5$ nm^{-1} for the 2 nm layer. As the layer width is reduced, the branches will therefore converge at higher k. Moreover, because of the higher contribution from the symmetric branch, this explains the shift of the IP feature to higher energies for the 2 nm SiO_2 layer [Fig. 2(b)].

As the layer width is reduced even further, the delocalized effects discussed above will be amplified. Taking the limit of Eq. (3) when the layer width d goes to 0, we obtain

$$\chi_{d\to 0} = \chi_{\text{bulk}}^{\text{Si}} + O(d), \tag{4}$$

where in the classical limit ($c \to \infty$),

$$O(d) = \frac{d}{2}\left(\frac{\epsilon_{\text{SiO}_2}}{\epsilon_{\text{Si}}^2} - \frac{1}{\epsilon_{\text{SiO}_2}}\right).$$

In this first-order approximation, the symmetric mode is found to dominate the loss signal. This explains why the antisymmetric mode is barely visible in the simulated loss image of Fig. 9(b). More importantly, when the layer width is reduced, the whole spectrum is expected to converge toward the one for bulk Si.

V. CONCLUSION

Spatially resolved valence electron energy-loss spectra acquired in Si/SiO_2/poly-Si gate stacks vary considerably depending on the SiO_2 layer width. Most of the observed variations are explained with a local dielectric model using as inputs the bulk optical constants of Si and SiO_2. This approach accounts for the interaction between collective interface modes and includes relativistic effects, which need to be considered for an accurate interpretation of experimental spectra. When the electron probe is located in the SiO_2 layer, the model predicts delocalized contributions not only from the coupled Si/SiO_2 interface plasmons, but also from Čerenkov radiation and interband transitions associated with the neighboring Si media. As the layer width is reduced to 2 nm, low-loss spectra acquired in SiO_2 start to resemble the bulk Si spectrum due to the delocalized nature of these excitations. The features characteristic of bulk SiO_2 are lost. A limit on the possibility to directly extract local optical properties is set by these delocalization effects.

ACKNOWLEDGMENTS

This research was supported by the Semiconductor Research Corporation and the Cornell Center for Materials Research, an NSF MRSEC. The authors are grateful to John Grazul for technical support and maintenance of the facilities.

*m.couillard@cornell.edu

[1] See *The International Technology Roadmap for Semiconductors*, Semiconductor Industry Association; see also http://public.itrs.net/ for the most recent updates, 2005.
[2] D. A. Muller, T. Sorsch, S. Moccio, F. H. Baumann, K. Evans-Lutterodt, and G. Timp, Nature (London) **399**, 758 (1999).
[3] P. E. Batson, Nature (London) **366**, 727 (1993).
[4] M. P. Agustin, G. Bersuker, B. Foran, L. A. Boatner, and S. Stemmer, J. Appl. Phys. **100**, 024103 (2006).
[5] M. Couillard, M.-S. Lee, D. Landheer, X. Wu, and G. A. Botton, J. Electrochem. Soc. **152**, F101 (2005).
[6] B. Foran, J. Barnett, P. S. Lysaght, M. P. Agustin, and S. Stemmer, J. Electron Spectrosc. Relat. Phenom. **143**, 149 (2005).
[7] A. J. Craven, M. MacKenzie, D. W. McComb, and F. T. Docherty, Microelectron. Eng. **80**, 90 (2005).
[8] G. D. Wilk and D. A. Muller, Appl. Phys. Lett. **83**, 3984 (2003).
[9] H. Raether, *Excitation of Plasmons and Interband Transitions by Electrons* (Springer-Verlag, Berlin, 1980).
[10] M. Couillard, M. Kociak, O. Stéphan, G. A. Botton, and C. Colliex, Phys. Rev. B **76**, 165131 (2007).
[11] H. Komoda, A. Watada, K. Ishida, K. Sasakawa, T. Okano, Y. Tsubokawa, and M. Terauchi, Jpn. J. Appl. Phys., Part 1 **40**, 4512 (2001).
[12] P. Moreau, N. Brun, C. A. Walsh, C. Colliex, and A. Howie, Phys. Rev. B **56**, 6774 (1997).
[13] M. A. Turowski, T. F. Kelly, and P. E. Batson, J. Appl. Phys. **76**, 3776 (1994).
[14] M. G. Walls and A. Howie, Ultramicroscopy **28**, 40 (1989).
[15] M. C. Cheynet and T. Epicier, Philos. Mag. **84**, 1753 (2004).
[16] H. Fukuda, M. Yasuda, and T. Iwabuchi, Appl. Phys. Lett. **61**, 693 (1992).
[17] A. Howie, Micron **34**, 121 (2003).
[18] D. A. Muller and J. Silcox, Ultramicroscopy **59**, 195 (1995).
[19] N. Bohr, Philos. Mag. **25**, 10 (1913).
[20] J. D. Jackson, *Classical Electrodynamics* (Wiley, New York, 1999).
[21] H. Cohen, T. Maniv, R. Tenne, Y. Rosenfeld Hacohen, O. Stephan, and C. Colliex, Phys. Rev. Lett. **80**, 782 (1998).
[22] J. Nelayah, M. Kociak, O. Stéphan, M. Tencé, L. Henrard, D. Taverna, I. Pastoriza-Santos, L. M. Liz-Marzàn, and C. Colliex, Nat. Phys. **3**, 348 (2007).
[23] F. J. García de Abajo and A. Howie, Phys. Rev. B **65**, 115418 (2002).
[24] O. Stéphan, D. Taverna, M. Kociak, K. Suenaga, L. Henrard, and C. Colliex, Phys. Rev. B **66**, 155422 (2002).
[25] M. Kociak, O. Stéphan, L. Henrard, V. Charbois, A. Rothschild, R. Tenne, and C. Colliex, Phys. Rev. Lett. **87**, 075501 (2001).
[26] P. E. Batson, K. L. Kavanagh, J. M. Woodall, and J. W. Mayer, Phys. Rev. Lett. **57**, 2729 (1986).
[27] L. Gu, V. Srot, W. Sigle, C. Koch, P. van Aken, F. Scholz, S. B. Thapa, C. Kirchner, M. Jetter, and M. Ruhle, Phys. Rev. B **75**, 195214 (2007).
[28] R. Arenal, O. Stéphan, M. Kociak, D. Taverna, A. Loiseau, and C. Colliex, Phys. Rev. Lett. **95**, 127601 (2005).
[29] J. P. R. Bolton and M. Chen, J. Phys.: Condens. Matter **7**, 3373 (1995); **7**, 3389 (1995); **7**, 3405 (1995); and Ultramicroscopy **60**, 247 (1995).
[30] E. N. Economou, Phys. Rev. **182**, 539 (1969).
[31] M. Stöger-Pollach and P. Schattschneider, Ultramicroscopy **107**, 1178 (2007).
[32] R. Erni and N. D. Browning, Ultramicroscopy **108**, 84 (2007).
[33] S. Lazar, G. A. Botton, and H. W. Zandbergen, Ultramicroscopy **106**, 1091 (2006).
[34] M. Stöger-Pollach, H. Franco, P. Schattschneider, S. Lazar, B. Schaffer, W. Grogger, and H. W. Zandbergen, Micron **37**, 396 (2006).
[35] F. J. García de Abajo, N. Zabala, A. Rivacoba, A. G. Pattantyus-Abraham, M. O. Wolf, and P. M. Echenique, Phys. Rev. Lett. **91**, 143902 (2003).
[36] F. J. García de Abajo, A. Rivacoba, N. Zabala, and N. Yamamoto, Phys. Rev. B **69**, 155420 (2004).
[37] C. H. Chen, J. Silcox, and R. Vincent, Phys. Rev. B **12**, 64 (1975).
[38] E. Kröger, Z. Phys. **235**, 403 (1970).
[39] E. Kröger, Z. Phys. **216**, 115 (1968).
[40] R. F. Egerton, *Electron Energy-Loss Spectroscopy in the Electron Microscope* (Plenum, New York, 1996).
[41] J. Aizpurua, A. Howie, and F. J. García de Abajo, Phys. Rev. B **60**, 11149 (1999).
[42] P. M. Echenique, Philos. Mag. B **52**, L9 (1985).
[43] G. Gumbs and N. J. M. Horing, Phys. Rev. B **43**, 2119 (1991).
[44] E. Fermi, Phys. Rev. **57**, 485 (1940).
[45] E. D. Palik, *Handbook of Optical Constants* (Academic, Orlando, 1998).
[46] R. García-Molina, A. Gras-Martí, A. Howie, and R. H. Ritchie, J. Phys. C **18**, 5335 (1985).
[47] R. H. Ritchie, Phys. Rev. **106**, 874 (1957).